Bit-Error-Rate Analysis of UWB Radio Using BPSK Modulation over Inter-Chip Radio Channels for Wireless Chip Area Networks

Zhiming Chen, *Student Member, IEEE,* Yue Ping Zhang, Ai Qun Hu, *Member, IEEE*, and Tung-Sang Ng, *Fellow, IEEE*

***Abstract*—Wireless chip area networks (WCAN) signify a new development in wireless communications, where wireless interconnections among different cores within a chip (intra-chip) or among different chips within a module (inter-chip) can be realized. In this paper, we analyze bit-error rate (BER) of an ultra-wideband (UWB) radio with binary phase-shift keying (BPSK) modulation over an inter-chip wireless radio channel. Specifically, a novel technique of dynamically shifting an integral window is proposed to reduce the effects of inter-symbol interference (ISI). BER expressions are analytically derived and verified by Monte Carlo simulations. Furthermore, by including both thermal and switching noise as the dominant noise sources, it is found that a BER less than 10^{-6} is feasible for a link distance up to 252 mm at a data rate of up to 650 Mbps. Besides, the link margin analysis shows that a link margin of 28.22 dB could be obtained for the same distance and data rate.**

***Index Terms*—Wireless chip area networks, inter-chip, bit-error rate, binary phase-shift keying.**

I. Introduction

In long-range systems, a wireless network covers a distance on the order of kilometers with a data rate of hundreds of kbps. The data rate increases with a shrinkage in the coverage range. In short-range systems, a wireless network is able to support a high rate on the order of tens of Mbps. For example, the wireless local area network (WLAN) standard 802.11g can cover an indoor distance around 30 meters up to 54 Mbps as released in June 2003 [1]. As the communication distance reduces to a few meters, the data rate rockets up to 600 Mbps [2]. From the range-speed relationship in the evolution of wireless communications, it can be deduced that with a sub-meter coverage, the communication speed can be further improved, i.e., to Gbps.

UWB technology emerges as a promising candidate for low-cost, high-performance and short-range applications. With a minimum fractional bandwidth 20% or absolute bandwidth 500 MHz, the maximum allowed effective isotropic radiated power (EIRP) is -41.3 dBm/MHz within the allocated frequency range from 3.1 to 10.6 GHz [3]. For an impulse radio, such a wide bandwidth can be realized by transmitting extremely narrow pulses at very low power spectral density (PSD). With a huge bandwidth and a narrow pulse width, the UWB technology features a variety of competitive advantages: low probability of detection and interception, high resolution capability, through-obstacle penetrating capability and robustness over multipath channels [4], [5]. Therefore, UWB is suitable for indoor high-rate data communications, low-rate data communications and accurate ranging.

In the semiconductor industry, the device feature dimension has been continuously scaled down to allow more transistors to be integrated into the same chip and to improve device performance. Furthermore, the chip size continues increasing at the same time such that more functions can be integrated into the same chip. However, as the width and thickness of wire interconnects are scaled down in proportion to the device feature dimension, the down scaling leads to problems of wire interconnects, especially at high frequencies, e.g., increased time delay, signal attenuation and dispersion, degraded bit-capacity, crosstalk, etc [6], [7]. To tackle the problems of wire interconnects in the age of high-speed semiconductor technology, WCAN proposed by Zhang is an innovative application which provides high data rates in close proximity [8], [9]. Apart from the application as an alternative for wire interconnects, a short-range high data rate link can be used to monitor and to diagnose computer systems as well [10]. Wireless interconnects can be used in concurrency with wire interconnects as a backup communication channel when mission-critical applications are running. An intra-chip BER evaluation and an inter-chip demonstration have been performed [9], [11]. In order to fully explore the capacity of wireless inter-chip channels, frequency domain data were sampled inside computer enclosures over 3.1 to 10.6 GHz for inter-chip channels and converted into the time domain using Inverse Discrete Fourier Transform (IDFT). Channel characteristics were obtained based on statistical modeling [12].

Manuscript received May 17, 2007; revised November 14, 2007, May 19, 2008, August 30, 2008, and December 24, 2008; accepted January 24, 2009. The associate editor coordinating the review of this paper and approving it for publication was T. A. Gulliver.

Z. M. Chen was with the School of Electrical and Electronic Engineering, Nanyang Technological University, Singapore 639798. He is now with the Integrated Circuits and Systems Laboratory, Institute of Microelectronics, 11 Science Park Road, Science Park II, Singapore 117685 (e-mail: chenzm@ime.a-star.edu.sg).

Y. P. Zhang is with the School of Electrical and Electronic Engineering, Nanyang Technological University, Singapore 639798 (e-mail: eypzhang@ntu.edu.sg).

A. Q. Hu is with Southeast University, China (e-mail: aqhu@seu.edu.cn).

T. S. Ng is with the University of Hong Kong, Hong Kong (e-mail: tsng@eee.hku.hk).

This work was partially supported by the Research Grant Council of Hong Kong under Project HKU 7165/05E.

Digital Object Identifier 10.1109/TWC.2009.070518

As there are dense multipaths in inter-chip channels, ISI becomes a significant performance-limiting factor. Conventionally, ISI can be reduced by using orthogonal frequency-division multiplexing (OFDM) in a multi-carrier communication system [13], [14], or using various equalizers in pulse-based systems [15]–[18]. In this paper, a relatively simple algorithm is proposed to reduce ISI in an impulse-based UWB radio. More importantly, for a transceiver to be designed to fully explore the radio channel capacity, it is necessary to perform a BER analysis to find out the supported data rates. Therefore, based on the inter-chip wireless channel modeled in [12], we analyze the BER for practical communication scenarios by taking various noise sources into consideration.

This paper is organized as follows. Section II provides a brief description for the modeled inter-chip wireless radio channel. In Section III, the communication system model is described. The proposed ISI reduction technique is presented in Section IV. Based on the proposed ISI-reduction technique, analytical expressions and numerical results of the BER analysis for inter-chip channels are derived in Section V. Finally, remarking conclusions are drawn in Section VI.

II. Inter-Chip Wireless Radio Channel

To obtain the statistical characteristics of a wireless inter-chip channel, data collection was performed in a typical commercial COMPAQ personal computer, where typical components such as an independent graphic card, memory chips, a hard drive, a floppy drive and a zip drive were installed [12]. A pair of UWB antennas [11], whose impedance bandwidth covers the 3.1-10.6 GHz band, were adopted for the channel measurement on a workbench in a typical laboratory. The collected data were recorded in an Agilent PNA-L network analyzer of the model N530A up to 20 GHz. With both scenarios of line-of-sight (LOS) and non-LOS (NLOS) included, the data sampling was performed in the frequency domain over UWB 3.1 to 10.6 GHz and the time-domain data were obtained using IDFT, resulting in sets of data with a time-domain resolution $1/(2B)$, where B is the measurement frequency span. The channel measurement covered a transmitter-receiver (T-R) distance from 62 to 252 mm. In the large-scale analysis, path loss is described by

$$PL = \gamma 10 \log_{10}(d/d_0) + PL_0 + X_\sigma \tag{1}$$

where PL is the path loss, which gives the power attenuation in dB at distance d. γ, d_0, and PL_0 are the path loss factor, reference distance and interception point of the model-fitted line with the vertical power axis, respectively. The factor X_σ is a zero-mean Gaussian random variable in dB with a standard deviation σ. Parameters for the large-scale analysis are shown in Table I for both closed and open computer casings.

When the computer casing is closed, negligible energy escapes out of the metal boundary, resulting in a rich-multipath environment and therefore a lower path loss factor. However, the rich multipath gives a channel impulse response (CIR) with a long delay spread as well. The average delay spread over local measurements can be up to 1.8659 ns when the computer casing is closed. One important observation is that the exponential path loss model underestimates the received energy due to reactive coupling if an antenna is placed too close to the metal casing, e.g., 7 mm. To avoid the reactive coupling or a short circuit to the metal case, antenna placements in such manners are undesirable. In the small-scale analysis, the lognormal distribution, characterized by mean μ and standard deviation σ, is found as the best-fitted for the computer casing both closed and open. Both μ and σ follow normal distributions with different sets of parameters. For the scenario of a closed computer casing, μ and σ of the lognormal distribution are described by normal distributions with parameters $N(\mu\_\mu, \sigma\_\mu)$ and $N(\mu\_\sigma, \sigma\_\sigma)$, respectively. Both sets of parameters are dependent on the T-R separation distance d in mm as

$$\mu\_\mu = 0.009741 \times d - 2.313 \tag{2a}$$

$$\sigma\_\mu = -0.004473 \times d + 1.909 \tag{2b}$$

$$\mu\_\sigma = -0.006687 \times d + 5.239 \tag{2c}$$

$$\sigma\_\sigma = -0.003702 \times d + 1.631 \tag{2d}$$

Similarly, when the computer casing is open, mean μ' and standard deviation σ' of the lognormal distribution are described by another two sets of distance-dependent normal distribution parameters [12]. As an illustration, experimental and simulated power delay profiles (PDPs) are depicted in Fig. 1 at an average T-R separation of 228 mm for the closed computer casing.

In order to make sure that the channel is sampled in a representative environment for wireless inter-chip communications, measurement points were selectively sampled in a Ranger WorkHorse commercial computer of a different size and a different internal configuration with a different external environment. It has been found that for path loss, the verification data were close to values predicted by the fitted model within 2 dB and 5 dB for the computer casing closed and open, respectively. The larger deviation for the open casing is due to differences in both the internal configuration and the surrounding environment. The consistency between the fitted model and the verification data makes the modeling work a typical inter-chip radio channel.

TABLE I
Path Loss Parameters.

	Casing closed	Casing open
γ	1.607	2.692
$d_0(mm)$	62	62
$PL_0(dB)$	23.78	25.27
$\sigma(dB)$	0.5482	1.9088

III. System Description

With the BPSK modulation adopted in the evaluation of BER performance for intra-chip interconnect systems and the design for wireless inter-chip interconnects [9], [11], we consider the same modulation scheme in this paper. Fig. 2 shows the block diagram of the inter-chip wireless communication system under consideration. The modulating signal $\{d_j\}_{j=-\infty}^{\infty}$ is an independent and identically distributed (iid) random

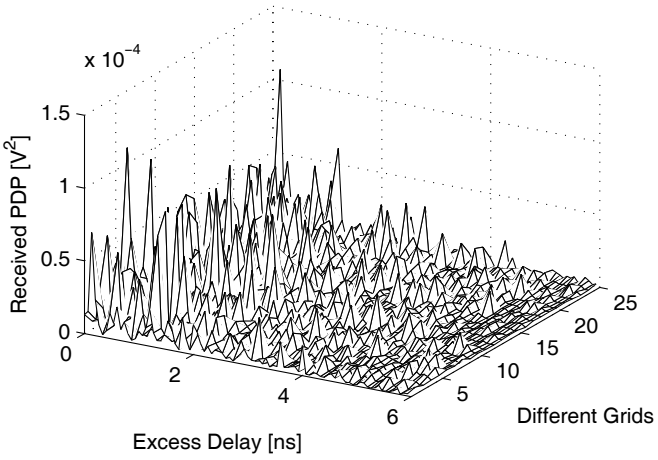

(a) The generated small-scale PDPs for the casing closed at 228 mm.

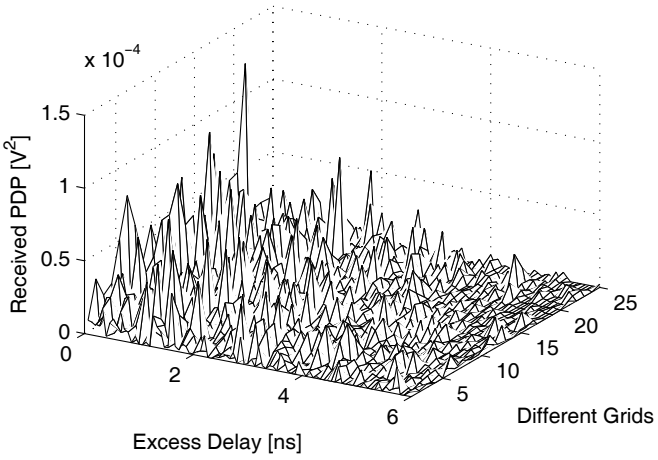

(b) The experimental small-scale PDPs for the casing closed at 228 mm.

Fig. 1. The generated and experimental small-scale PDPs at 228 mm.

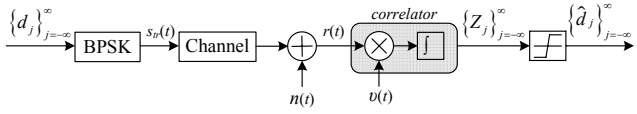

Fig. 2. The block diagram for an inter-chip wireless communication system.

variable and can be '0' or '1' for binary signalling. Through the modulator of BPSK, the transmitted signal $s_{tr}(t)$ can be expressed as

$$s_{tr}(t) = \sum_{j=-\infty}^{\infty} \sqrt{A}\beta_j \omega_{tr}\left(t - jT_f\right) \tag{3}$$

where T_f is the pulse repetition frame time and $\omega_{tr}(t)$ is the energy normalized transmitted pulse with a duration T_m. A is to adjust the transmitted power. The modulation signal β_j for the jth pulse has a mapping with the source signal d_j as

$$\beta_j = 2 \times d_j - 1 = \begin{cases} -1, & d_j = 0 \\ +1, & d_j = 1 \end{cases}. \tag{4}$$

The channel impulse response $h(t)$, including the effects of both transmitting and receiving antennas, can be expressed as

$$h(t) = \sum_{l=0}^{L-1} \alpha_l \delta\left(t - \tau_l\right) \tag{5}$$

where α_l and τ_l are the signal attenuation and delay for the lth path. $\delta(t)$ is the Dirac delta function and L is the total number of multipaths present.

The received signal at the input of the receiver correlator can be obtained as

$$\begin{aligned} r(t) &= s_{tr}(t) \otimes h(t) + n(t) \\ &= \sum_{j=-\infty}^{\infty} \sqrt{A}\beta_j \omega_{rec}\left(t - jT_f - \tau_d\right) + n(t) \end{aligned} \tag{6}$$

where τ_d is the propagation delay between the transmitter and receiver involved and $n(t)$ is the additive white Gaussian noise (AWGN) characterized by mean zero and two-sided PSD $N_0/2$. The notation $\otimes$ denotes the convolution operation. $\omega_{rec}(t)$ is the received pulse waveform including effects of the communication channel and both antennas

$$\begin{aligned} \omega_{rec}\left(t - \tau_d\right) &= \omega_{tr}\left(t - jT_f\right) \otimes h(t) \\ &= \sum_{l=0}^{L-1} \alpha_l \omega_{tr}\left(t - jT_f - \tau_l\right). \end{aligned} \tag{7}$$

By assuming that perfect knowledge of the communication channel has been obtained, the decision variable Z_j at a synchronized receiver can be obtained as

$$Z_j = \int_{\tau_r + (j-1)T_f}^{\tau_r + jT_f} r(t)\upsilon(t)\, dt \tag{8}$$

where τ_r is the receiver time reference and $\upsilon(t)$ is the locally generated mask signal to be correlated with the received signal. The decision variable Z_j is then fed into a comparator to perform estimations of the transmitted bits $\{\widehat{d}_j\}_{j=-\infty}^{\infty}$ according to

$$\widehat{d}_j = \begin{cases} 0, & Z_j < 0 \\ 1, & Z_j > 0 \end{cases}. \tag{9}$$

IV. ISI Reduction

The transmitted basic pulse is chosen as a polypulse described by

$$\omega_{tr}(t) = \frac{1}{\sqrt{E_p}} \sin\left(2\pi f_e t\right) \sin\left(2\pi f_c t\right) \tag{10}$$

where $f_e = 1/T_e$ and $f_c = 1/T_c$ are the envelope and carrier frequencies, respectively. E_p is to normalize the energy of the pulse to unity. The duration of the pulse is limited by $t \in [0, T_e/2]$. In order to meet requirements of the FCC UWB emission mask and a high data rate, we set $T_e = 0.75$ ns and $T_c = 0.15$ ns. With this polypulse, the -10 dB cut-off frequencies are at 3.9793 and 9.6166 GHz respectively, leading to a -10 dB bandwidth of 5.6373 GHz.

The correlator mask signal at the receiver can be written as

$$v(t) = \sum_{j=-\infty}^{\infty} \omega_{cor}\left(t - jT_f - \tau_r\right) \tag{11}$$

where $\omega_{cor}(t)$ a energy-normalized pulse waveform used for correlation. With an All-RAKE receiver implementation, $\omega_{cor}(t)$ is the same as $\omega_{rec}(t)$. Therefore, from (8), the decision variable Z_j for the jth pulse can be expanded as

$$\begin{aligned} Z_j &= \int_{\tau_r+(j-1)T_f}^{\tau_r+jT_f} \left[\sum_{j=-\infty}^{\infty} \sqrt{A}\beta_j \omega_{rec}\left(t - jT_f - \tau_d\right) + n(t)\right] \\ &\quad \times v(t)\, dt \\ &= \sum_{m=-\infty}^{j-1} \sqrt{A}\beta_m \int_{\tau_r+(j-1)T_f}^{\tau_r+jT_f} \omega_{rec}\left(t - mT_f - \tau_d\right) \\ &\quad \times v(t)\, dt \\ &\quad + \sqrt{A}\beta_j \int_{\tau_r+(j-1)T_f}^{\tau_r+jT_f} \omega_{rec}\left(t - jT_f - \tau_d\right) \times v(t)\, dt \\ &\quad + \int_{\tau_r+(j-1)T_f}^{\tau_r+jT_f} n(t) \times v(t)\, dt \\ &= Z_{j,ISI} + Z_{j,D} + Z_{j,n} \end{aligned} \tag{12}$$

where $Z_{j,ISI}$, $Z_{j,D}$ and $Z_{j,n}$ are the contributions in Z_j from ISI, the desired signal and Gaussian noise. With the channel length denoted as T_{ch}, which is determined by the first and last arrivals above noise floor, a metric k can be defined to quantify the severity of ISI

$$k = \lceil (T_m + T_{ch})/T_f \rceil \tag{13}$$

where $\lceil x \rceil$ rounds x up to the nearest integer. $k-1$ gives the number of preceding pulses, whose residuals affect the decision of the jth pulse, when $j \geq k$. Therefore the ISI-contributed term in Z_j can be rewritten as

$$\begin{aligned} Z_{j,ISI} = \sum_{m=j-k+1}^{j-1} \sqrt{A}\beta_m \int_{\tau_r+(j-1)T_f}^{\tau_r+jT_f} \omega_{rec}(t - mT_f - \tau_d) \\ \times v(t)\, dt \end{aligned}. \tag{14}$$

The ISI term $Z_{j,ISI}$ will be non-zero with the value of k greater than unity. If the residuals of the preceding $k-1$ bits are strong enough, a wrong estimation of the jth transmitted pulse may be resulted. For different values of j, the number of preceding pulses, which affect the jth pulse, can be expressed as

$$\begin{cases} k-1, & j \geq k \\ j-1, & j \leq k-1 \end{cases}. \tag{15}$$

To illustrate the effects of residuals from the preceding pulses on the pulse under consideration, Fig. 3 depicts the mixer output with $k = 5$. The vertical lines indicate bit intervals in Fig. 3, where T_{ch} is less than 6 ns and T_f is the reciprocal of the data rate of 650 Mbps. The transmitted bits are 101010. Therefore, the correlator output should be

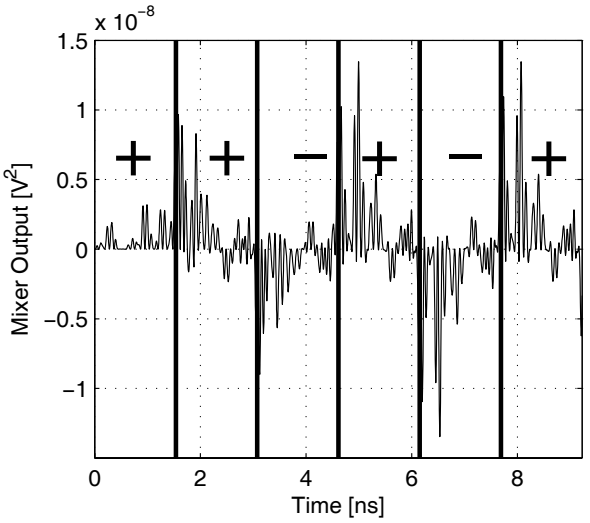

Fig. 3. An example for effects of ISI.

$+-+-+-$ for correct decision makings. However, the obtained results are $++-+-+$, i.e., all the received bits are incorrectly estimated except for the first bit where there is no ISI.

Conventionally, ISI problems can be alleviated using approaches of OFDM techniques in a multi-carrier system [13], [14] or various equalizers in pulse-based systems [15]–[18]. For the adopted polypulse, the received signal preserves the same zero-crossing rate as the mask signal except at transitions in the successively transmitted bits. The zero-crossing rate refers to the frequency at which a signal crosses the x axis. As the transmitted signal passes through a multipath radio channel, the received signal is actually a sum of replicas of the transmitted signals with different delays and gains. The transmitted signal is a sinusoidal signal with an envelope as half a period of another sinusoidal signal. Therefore, the added replicas still possess the same zero-crossing rate but with different phases and gains, as compared to the transmitted signal. A transition in the consecutively transmitted bits will result in a distorted zero-crossing rate in $r(t)$ with respect to the mask signal $v(t)$ due to the residual of the preceding bit with a different sign, and therefore affect the decision making. In other words, if the consecutively transmitted bits are the same, the decision making will be correct even when there is ISI.

On the other hand, it is known that the received energy generally decays exponentially over time. Most of the received energy is actually confined in the beginning portion. Therefore, by finding an "optimal" position for the integral window, i.e., by adjusting τ_r in (8), the integral can be performed with a focus on the desired pulse whereas effects of the preceding and succeeding pulses can be limited to a very low level. More specifically, the receiver time reference τ_r can be broken into two parts as

$$\tau_r = \tau_d + \tau_{sh} \tag{16}$$

where τ_d is to account for the propagation delay between the transmitter and receiver, and τ_{sh} is to further dynamically search for the "optimal" integral window position. To avoid

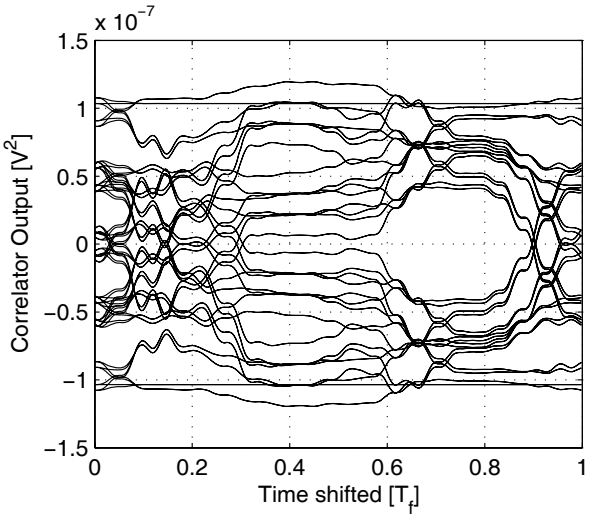

Fig. 4. $Z_{j,r}(\tau_{sh})$ over the time shift τ_{sh} for the jth pulse as '0' and '1'. τ_{sh} is in the unit of T_f.

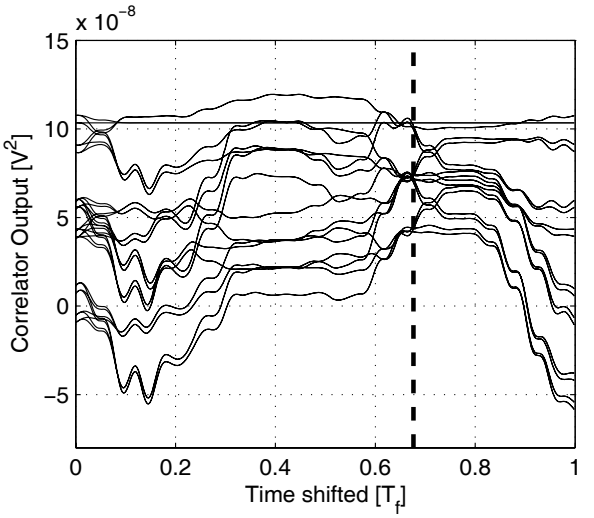

Fig. 5. $Z_{j,r}(\tau_{sh})$ over the time shift τ_{sh} for the jth pulse as '1'. τ_{sh} is in the unit of T_f. The vertical dashed line represents $\tau_{sh,opt}$.

distortions of many succeeding pulses, we limit the range of τ_{sh} as $\tau_{sh} \in [0, T_f)$. By denoting the decisional variable due to the received signal as $Z_{j,r} = Z_{j,ISI} + Z_{j,D}$, $Z_{j,r}$ is a function of $k+1$ pulses for $j \geq k$: the preceding $k-1$ pulses, the jth pulse under investigation and the $(j+1)$th pulse due to shifting of the integral window position. The maximum number of possible $Z_{j,r}$ can be derived as

$$P = \begin{cases} 2^{k+1}, & j \geq k \\ 2^{j+1}, & j \leq k-1 \end{cases}. \tag{17}$$

Fig. 4 depicts the function $Z_{j,r}(\tau_{sh})$ over the shifted time τ_{sh} with $k = 5$. In order to view the details about the effects of τ_{sh}, the simulation sampling frequency is set to 400 GHz. It can be observed that $Z_{j,r}(\tau_{sh})$ is symmetrical about the horizontal x axis. The symmetry corresponds to the balanced source signal $\{d_j\}_{j=-\infty}^{\infty}$. For instance, the modulating source sequences 101101 and 010010 are mirrors of each other and their $Z_{j,r}(\tau_{sh})$ will be symmetrical about the horizontal x axis. As the number P increases exponentially over k with base 2, it implies that the actual computation complexity could be reduced by half. As a result, from (17), the maximum number of possible $Z_{j,r}$ can be reduced to

$$P = \begin{cases} 2^{k}, & j \geq k \\ 2^{j}, & j \leq k-1 \end{cases}. \tag{18}$$

To obtain the optimal value of τ_{sh}, Fig. 5 gives the plot of $Z_{j,r}(\tau_{sh})$ when the jth pulse is for '1' and the vertical dashed line indicates the optimal time shift $\tau_{sh,opt}$. The desired correlator output is positive for a correct decision making. A more positive $Z_{j,r}(\tau_{sh})$ is preferred against noise during the decision making. Therefore, for the pth possible combination of the modulating source bits, where $p \in P$ as shown in (18), an algorithm for obtaining the optimal time shift $\tau_{sh,opt}$ can be described as

$$\tau_{sh,opt} = \arg\max_{\tau_{sh}} \left\{ \arg\min_{p} \{Z_r^p(\tau_{sh})\} \right\}. \tag{19}$$

More specifically, Fig. 6 gives a flow chart on how to find the $\tau_{sh,opt}$, where $\Delta\tau_{sh}$ is the search resolution. For different values of p, the minimum values of $Z_r^p(\tau_{sh})$ at each τ_{sh} are stored in buffer 2. The maximum value in buffer 2 corresponds to the position of $\tau_{sh,opt}$. How close to theoretical maximum for the actually obtained $\tau_{sh,opt}$ depends on the shifting resolution during the searching process for the optimum integral window position. Besides, if there is a relatively flat region near the $\tau_{sh,opt}$ point as the segment of $0.65T_f$ to $0.8T_f$ in Fig. 5, the requirement on the search resolution $\Delta\tau_{sh}$ could be relaxed. As in (16), ideal synchronization between the transmitter and receiver has been assumed. In practice, synchronization is important to the receiver performance since τ_d gives the starting point to shift the integral window position. Techniques such as phase-locked loops (PLL) or delay locked loops (DLL) can be utilized to achieve accurate synchronization between the transmitter and receiver [19]. However, if the flat portion in Fig. 5 is relatively large, the requirement on synchronization can be relaxed. Furthermore, it should be noted that scaling the mask signal $v(t)$ with a constant does not change the sign of $Z_{j,r}$. Therefore, for a transmitted bit as '1', any constantly negative $Z_{j,r}(\tau_{sh})$ over the entire range of τ_{sh} indicates an error decision, which cannot be solved by the proposed technique of shifting the integral window position. The error decision is caused by the overlapping of successively transmitted pulses, leading to uncontrollable ISI and resulting in an error floor in the BER. In this case, the solution is to lower the transmission bit rate or use other means to reduce the ISI. It is worthwhile mentioning that apart from the BPSK modulation scheme, the technique of dynamically shifting the integral window position has been verified in the binary pulse-position modulation (PPM) scheme as well.

V. BER Analysis Over Inter-Chip Channels

For certain combination of the transmitted modulating source bits, the bit error probability $P_{e,j}$ can be expressed as a function of Z_j

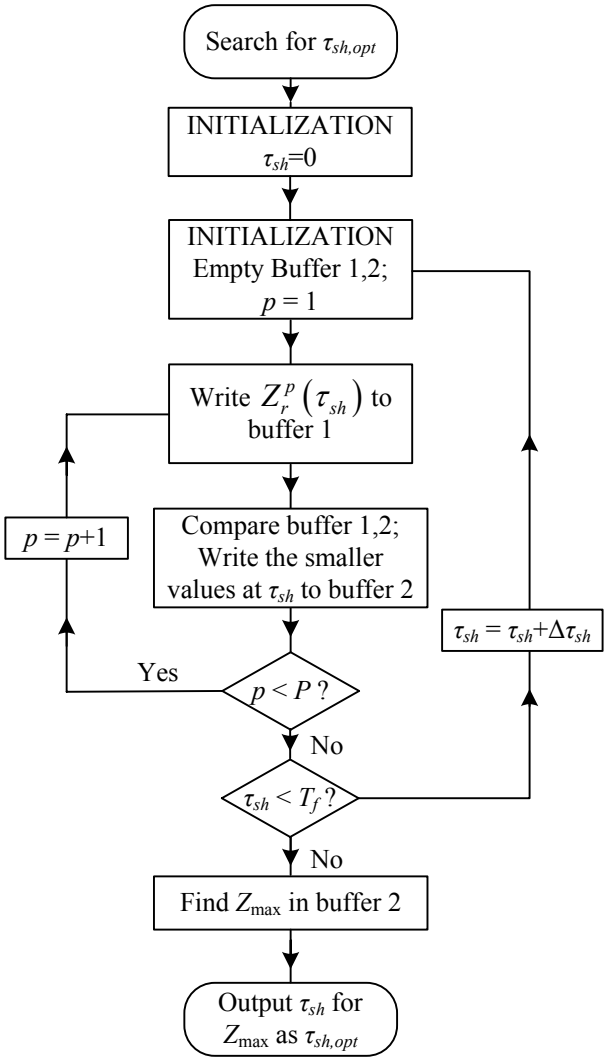

Fig. 6. Flow chart for $\tau_{sh,opt}$ searching.

$$P_{e,j} = Q\left(\frac{E(Z_j)}{std(Z_j)}\right) \tag{20}$$

where $E(x)$ gives the expected value of x and std the standard deviation. The Q function is defined as

$$Q(x) = \frac{1}{\sqrt{2\pi}}\int_x^{\infty} e^{-t^2/2}\,dt. \tag{21}$$

From (12) and (14), $E(Z_j)$ can be obtained as

$$\begin{aligned} E(Z_j) &= E\left(\sum_{m=j-k+1}^{j+1}\sqrt{A}\beta_m r_m(t)\right) \\ &\quad + E\left(\int_{\tau_d+\tau_{sh,opt}+(j-1)T_f}^{\tau_d+\tau_{sh,opt}+jT_f} n(t)\times \upsilon(t)\,dt\right). \\ &= \sum_{m=j-k+1}^{j+1}\sqrt{A}\beta_m r_m(t) \end{aligned} \tag{22}$$

where $r_m(t)$ can be expressed as

$$r_m(t) = \int_{\tau_d+\tau_{sh,opt}+(j-1)T_f}^{\tau_d+\tau_{sh,opt}+jT_f} \omega_{rec}(t-mT_f-\tau_d)\times\upsilon(t)\,dt. \tag{23}$$

And the variance of Z_j can be derived as

$$\begin{aligned} Var(Z_j) &= Var\left(\sum_{m=j-k+1}^{j+1}\sqrt{A}\beta_m r_m(t)\right) \\ &\quad + Var\left(\int_{\tau_d+\tau_{sh,opt}+(j-1)T_f}^{\tau_d+\tau_{sh,opt}+jT_f} n(t)\times\upsilon(t)\,dt\right) \\ &= \frac{N_0}{2}R_{\upsilon\upsilon}(0) \end{aligned} \tag{24}$$

where $R_{\upsilon\upsilon}(\tau)$ is the auto-correlation function of the reference mask signal $\upsilon(t)$.Therefore, the general probability of error for the jth received pulse can be written as

$$P_{e,j} = \frac{1}{P}\sum_{i=1}^{P} Q\left(\frac{E(Z_{j,i})}{std(Z_{j,i})}\right) \tag{25}$$

where P is defined in (18). In the case when the total number of bits transmitted is N, the probability of a bit error can be obtained as

$$P_e = \frac{1}{N}\sum_{i=1}^{N} P_{e,i}. \tag{26}$$

The Q function in (25) can be re-written in the form of transmitted bit energy and the noise PSD $N_0/2$. The received signal amplitude is proportional to the square root of the transmitted bit energy E_{TX}

$$Amp(r(t)) = B\sqrt{E_{TX}} \tag{27}$$

where B is an unknown channel-dependent constant. Meanwhile, $E(Z_j)$ is in proportion to the received signal amplitude as in (22)

$$E(Z_j) = C\times Amp(r(t)) \tag{28}$$

where C is another channel-dependent constant. Combining (27) and (28)

$$\begin{aligned} E(Z_j) &= C\times B\times\sqrt{E_{TX}} \\ &= D\sqrt{E_{TX}} \end{aligned}. \tag{29}$$

D is the product of B and C, and dependent on the particular channel condition as B and C. As from (6) and (22), the value of D is determined by two factors: the received signal energy and the ISI effect. These relationships will be verified by the BER performance over the changes in the T-R distance and the data rate later. Therefore the Q function in (25) can be modified as

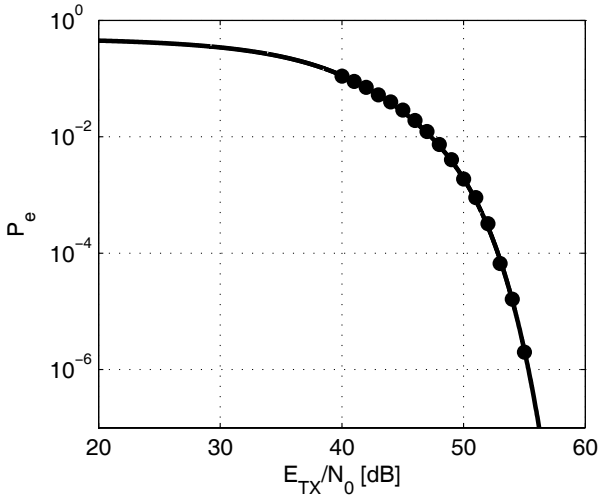

Fig. 7. Theoretical BER plot (solid line) and Monte Carlo verification (solid dot) at T-R separation of 228 mm.

$$Q\left(\frac{E(Z_j)}{std(Z_j)}\right) = Q\left(\frac{D_j\sqrt{E_{TX}}}{\sqrt{(N_0/2)R_{vv}(0)}}\right) = Q\left(\sqrt{\frac{E_{TX}}{N_0}}\frac{D_j}{\sqrt{0.5R_{vv}(0)}}\right). \quad (30)$$

The constant D can be obtained for each combination of the modulation source bits. The total number of D can be obtained from (18) as $\sum_{i=1}^{k} 2^i = 2(2^k - 1)$. For the inter-chip channel with $k = 5$, only 372 bits are required to determine the optimal shift time $\tau_{sh,opt}$.

By observing (26), the BER performance is a function of the number of bits transmitted. However, through calculation, it is found that the probability of error is dominated by that of the kth when a large number of bits are transmitted. A negligible effect of N in BER performance is found for $N > 10$. In practical communications, the inequality can always be satisfied. The above BER analysis are verified by Monte Carlo simulations. Fig. 7 compares the theoretical BER curve in a solid line with the Monte Carlo results in solid dots for a wireless inter-chip channel at 228 mm with a data rate of 650 Mbps. To ensure the accuracy, the Monte Carlo simulations run up to 1.1×10^6 bits. An excellent matching between the solid-line curve and the solid dots validates the analytical BER expression.

For the application of wireless interconnects inside computer casings, the wireless propagation channel is shielded almost completely by the metal enclosure. The communication channel can be considered as quasi-static. Hence, the rate of channel estimation can be at a low level. Furthermore, co-channel interfering sources from the outside is negligible. In this case, we consider two major noise sources: thermal and switching noise. The thermal noise PSD can be calculated using

$$N_{0,Th} = k_B(T_{Ant} + T_0(F - 1)) \quad (31)$$

where k_B, T_{Ant}, T_0 and F are the Boltzmann constant, antenna temperature (taken as 320 K due to the hot environment), standard temperature (290 K), and noise factor. Noise figure (NF), the noise factor in dB, is around $5-8$ dB for a UWB receiver [20]. Therefore, the thermal noise PSD can be obtained as -165.91 dBm/Hz with an assumption that NF is 8 dB over the $3.1-10.6$ GHz band.

In order to obtain an estimation of the switching noise PSD, we use a monopole planar UWB antenna [11] to sample the noise spectrum while a computer is running at its full capacity. A leading-edge NEC dual-core commercial computer, with a CPU frequency 3.0 GHz, is used for measurement. The switching noise occurs at harmonics of the fundamental frequency 1.5 GHz. The 3rd to 7th harmonics fall into the range of 3.1 to 10.6 GHz. The 3rd harmonic at 4.5 GHz is recorded as -89.93 dBm whereas all other harmonics beyond the 3rd one fall below the noise floor and therefore cannot be detected. With the measured harmonics and the assumption that there is an ideal bandpass filter over 3.1 to 10.6 GHz at the receiver, the switching noise PSD S can be obtained as

$$S = \sum_i \sum_j \frac{\chi_{ij} A_{ij}^2}{2} / B_W \quad (32)$$

where χ_{ij} is the ith coupling factor from the jth switching noise source and A_{ij} is the amplitude of the ith harmonic from the jth switching noise source within the system bandwidth B_W [11]. Therefore, by spreading the switching noise over the frequency span of 3.1 to 10.6 GHz, the switching noise PSD S can be obtained as -188.58 dBm/Hz. In typical multi-chip modules, there is more than one switching noise source. However, the switching noise is usually 10 dB lower than the thermal noise even for integrated antennas, as the switching noise is common-mode in nature and it can be effectively suppressed by balanced antenna structures and differential circuit architectures [21]. When the antenna used for sampling is not integrated into chips, the measured switching noise is even lower. Combining both noise sources, the total noise PSD is obtained as $N_{0,n} = N_{0,Th} + S = -165.88$ dBm/Hz.

When the T-R propagation distance increases, the path loss increases logarithmically, leading to lower received bit energy. Fig. 8 shows BER curves for the T-R distances at 62, 84, 133, 156, 162, 208, and 252 mm along the BER deteriorating direction for a data rate of 650 Mbps. It can be observed that approximately 21 dB more energy is required to achieve the same BER performance (10^{-6}) for the largest T-R separation, as compared to the shortest one. For the bit rate of 650 Mbps, the transmitted power Pow in dBm is related to the transmitted bit energy E_{TX} in mJ in log scale by

$$Pow = E_{TX} - 10\log_{10}(T_f) = E_{TX} + 88.13. \quad (33)$$

As a result, the power-to-noise ratio Pow/N_0 varies from 129.03 to 150.11 dB over the variations of the T-R separation distances. With the noise PSD including both thermal and switching noise, the corresponding required transmitted power varies from -36.85 to -15.77 dBm if the desired BER performance is better than 10^{-6}.

Apart from the bit energy and T-R separation distance, BER

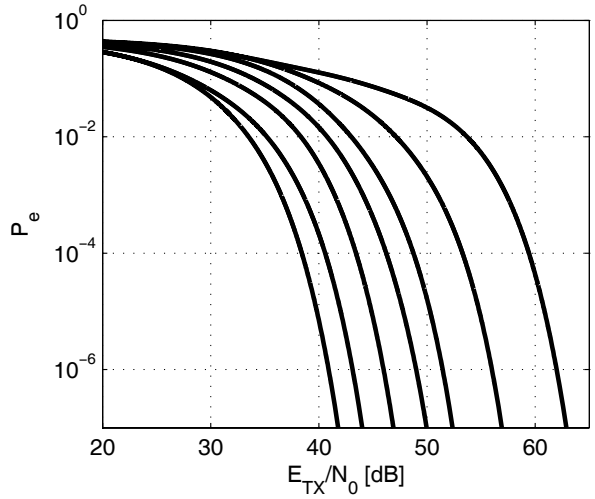

Fig. 8. BER over E_{TX}/N_0 over different distances at a data rate of 650 Mbps. The T-R distances are: 62, 84, 133, 156, 162, 208, and 252 mm.

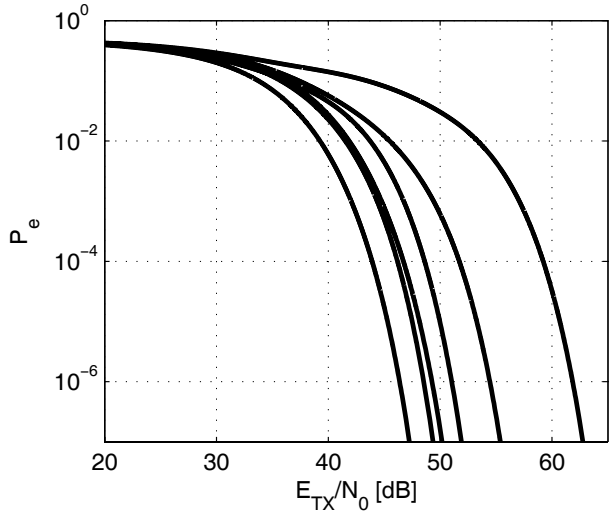

Fig. 9. BER over E_{TX}/N_0 over different data rates at T-R separation of 235 mm. Data rates: 450, 500, 550, 600, 650, and 700 Mbps.

performance is a function of the data rate as well. Lowering the data rate is to increase the frame time T_f. Correspondingly, k, the channel length in terms of the number of pulses, becomes small, which implies that fewer preceding bits have effects on the pulse under investigation. Generally, this leads to reduced ISI. Fig. 9 shows the BER plot over data rate at 450, 500, 550, 600, 650, and 700 Mbps along the BER worsening direction at a propagation distance of 235 mm. It can be observed that for the same CIR, a variation of approximately 15 dB in E_{TX}/N_0 is obtained when the bit rate is changed from 450 to 700 Mbps.

To obtain the insight of the power-performance relationship, it is necessary to perform a link budget analysis. Taking the longest distance 252 mm as an example, the required transmitted power Pow' is -15.77 dBm to achieve a BER lower than 10^{-6} for a data rate at 650 Mbps. The required transmitted power covers the path loss and gains of the transmitting and receiving antennas. Under the FCC regulations, the PSD of a transmitted UWB signal over 3.1 to 10.6 GHz can be up to -41.3 dBm/MHz, i.e., $P_{max} = -2.55$ dBm in total. The link margin G_m can be expressed as

$$G_m = P_{max} - Pow' + G_r \tag{34}$$

where G_r is the receiver gain, which is taken as 15 dB [11]. Therefore, the link margin is calculated as 28.22 dB. The implementation margin in [11] is assumed as 15 dB to cover the loss due to inevitable metal lines between the transmitter and receiver antennas and other marginal losses. The obtained high link margin G_m suggests that the transmitted power can be much lower than the maximum allowed transmitted power, though, in practice, the maximum transmitted power is always lower than the theoretical value of -2.55 dBm.

VI. Conclusion

BER analysis of a UWB radio using the BPSK modulation over inter-chip wireless channels has been performed. To reduce effects of ISI on the decision making at the receiver, the technique of dynamically shifting the integral window has been proposed. By dynamically shifting the integral window, an optimal position could be obtained for all possible combinations of residuals from preceding pulses. To obtain the BER performance over the wireless inter-chip channel, expressions have been derived analytically and verified by Monte Carlo simulations. It has been found that a BER less than 10^{-6} is feasible for the coverage distance from 62 to 252 mm at a data rate up to 650 Mbps. With thermal and switching noise as the dominant noise sources, the link budget has been analyzed and it has been found that a link margin of 28.22 dB could be obtained for the largest T-R separation at 252 mm with a data rate of 650 Mbps.

References

[1] IEEE Standard 802.11g, June 2003.
[2] J. P. Van't Hof and D. D. Stancil, "Ultra-wideband high data rate short range wireless links," in *Proc. IEEE Veh. Technol. Conf.*, vol. 1, pp. 85-89, May 2002.
[3] "In the matter of revision of part 15 of the commission's rules regarding ultra-wideband transmission systems," FCC, pp. 02-48, Apr. 2002.
[4] M. Z. Win and R. A. Scholtz, "Ultra-wide bandwidth time-hopping spread-spectrum impulse radio for wireless multiple acess communications," *IEEE Trans. Commun.*, vol. 48, no. 4, pp. 679-691, Apr. 2000.
[5] J.-Y. Lee and R. A. Scholtz, "Ranging in a dense multipath environment using an UWB radio link," *IEEE J. Select. Areas Commun.*, vol. 20, no. 9, pp. 1677-1683, Dec. 2002.
[6] M.-C. F. Chang, V. P. Roychowdhury, L. Zhang, H. Shin, and Y. Qian, "RF/wireless interconnect for inter- and intra-chip communications," *Proc. IEEE*, vol. 89, no. 4, pp. 456-466, Apr. 2001.
[7] R. J. Drost, R. D. Hopking, R. Ho, and I. E. Sutherland, "Proximity Communication," *IEEE J. Solid-State Circuits*, vol. 39, no. 9, pp. 1529-1535, Sept. 2004.
[8] M. Sun and Y. P. Zhang, "Performance of inter-chip RF-interconnect using CPW, capacitive coupler and UWB transceiver," *IEEE Trans. Microw. Theory Tech.*, vol. 53, no. 9, pp. 2650-2655, Sept. 2005.
[9] Y. P. Zhang, "Bit-Error-rate performance of intra-chip wireless interconnect systems," *IEEE Commun. Lett.*, vol. 8, no. 1, pp. 39-41, Jan. 2004.
[10] H. Eberle, "A radio network for monotoring and diagnosing computer systems," in *Proc. IEEE High Performance Interconnects*, Aug. 2002, pp. 135-139.
[11] Y. J. Zheng, Y. P. Zhang, and Y. Tong, "A novel wireless interconnect technology using impulse radio for inter-chip communications," *IEEE Trans. Microw. Theory Tech.*, vol. 54, no. 4, pp. 1912-1920, Apr. 2006.
[12] Z. M. Chen and Y. P. Zhang, "Inter-chip wireless communication channel: measurement, characterization, and modeling," *IEEE Trans. Antennas Propag.*, vol. 55, no. 3, pp. 978-986, Mar. 2007.

[13] R. v. Nee, *OFDM for Wireless Multimedia Communications*. Boston: Artech House, 2000.
[14] D. Gerakoulis and P. Salmi, "An interference suppressing OFDM system for ultra wide bandwidth radio channels," in *Proc. IEEE Ultra Wideband Systems Technologies*, May 2002, pp. 259-264.
[15] J. G. Proakis, *Digital Communications*, 4th ed. McGraw Hill, 2000.
[16] M. E. Sahin and H. Arslan, "Inter-symbol interference in high data rate UWB communications using energy detector receiver," in *Proc. IEEE ICUWB 2005*, Sept. 2005, pp. 176-179.
[17] R.-J. Chen, P. Chiu, and H.-L. Yang, "Design and performance analysis of DS-UWB rake receiver," in *Proc. IEEE ISCAS 2006*, May 2006, pp. 21-24.
[18] R.-J. Chen and C.-L. Tsai, "Design and performance analysis of the receiver for DS-UWB communication systems," in *Proc. IEEE ICUWB 2006*, Sept. 2006, pp. 651-656.
[19] Z. M. Chen and Y. P. Zhang, "A modified synchronization scheme for impulse-based UWB," in *Proc. IEEE ICICS2007*, Dec. 2007, pp. 1-5.
[20] G. Gusmai, M. Brandolini, P. Rossi, and F. Svelto, "A 0.18-μm CMOS selective receiver front-end for UWB applications," *IEEE J. Solid-State Circuits*, vol. 41, no. 8, pp. 1764-1771, Aug. 2006.
[21] B. A. Floyd, C.-M. Hung, and K. K. O, "Intra-chip wireless interconnect for clock distribution implemented with integrated antennas, receiver, and transmitters," *IEEE J. Solid-State Circuits*, vol. 37, no. 5, pp. 534-552, May 2002.

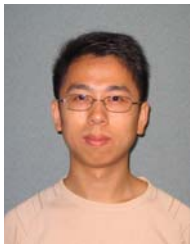

Zhiming Chen (S'04) was born in Jiangsu, China, in 1982. He received the B. Eng and Ph.D. degrees from Nanyang Technological University, Singapore, in 2005 and 2009, respectively, both in electrical and electronic engineering.

From 2008, he is with the Institute of Microelectronics, Singapore. His research interests include study of inter-chip wireless interconnect system and RF transceiver design for wireless communications.

Yue Ping Zhang received the B.E. and M.E. degrees from Taiyuan Polytechnic Institute and Shanxi Mining Institute of Taiyuan University of Technology, Shanxi, China, in 1982 and 1987, respectively and the Ph.D. degree from the Chinese University of Hong Kong, Hong Kong, in 1995, all in electronic engineering.

From 1982 to 1984, he worked at Shanxi Electronic Industry Bureau, from 1990 to 1992, the University of Liverpool, Liverpool, U. K., and from 1996 to 1997, City University of Hong Kong. From 1987 to 1990, he taught at Shanxi Mining Institute and from 1997 to 1998, the University of Hong Kong. He was promoted to a Full Professor at Taiyuan University of Technology in 1996. He is now an Associate Professor and the Deputy Supervisor of Integrated Circuits and Systems Laboratories with the School of Electrical and Electronic Engineering, Nanyang Technological University, Singapore. He has broad interests in radio science and technology and published widely across seven IEEE societies. He has delivered scores of invited paper/keynote address at international scientific conferences.

Prof. Zhang received the Sino-British Technical Collaboration Award in 1990 for his contribution to the advancement of subsurface radio science and technology. He received the Best Paper Award from the Second IEEE International Symposium on Communication Systems, Networks and Digital Signal Processing, 18-20th July 2000, Bournemouth, UK and the Best Paper Prize from the Third IEEE International Workshop on Antenna Technology, 21-23rd March 2007, Cambridge, UK. He was awarded a William Mong Visiting Fellowship from the University of Hong Kong in 2005. He is listed in Marquis Who's Who, Who's Who in Science and Engineering, Cambridge IBC 2000 Outstanding Scientists of the 21st Century.

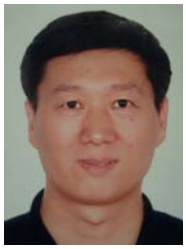

Ai Qun Hu received the B.Sc.(Eng.), the M.Eng.Sc. and Ph.D. degrees from Southeast University in 1987, 1990, and 1993 respectively.

He was invited as a post-doc research fellow in The University of Hong Kong from 1997 to 1998, and TCT fellow in Nanyang Technological University in 2006. His research interests include data transmission and secure communication technology. He has published two books and over 100 technical papers in wireless communications field.

Tung-Sang Ng received the B.Sc.(Eng.) degree from The University of Hong Kong in 1972, the M.Eng.Sc. and Ph.D. degrees from the University of Newcastle, Australia, in 1974 and 1977, respectively, all in electrical engineering.

He worked for BHP Steel International and The University of Wollongong, Australia after graduation for 14 years before returned to The University of Hong Kong in 1991, taking up the position of Professor and Chair of Electronic Engineering. He was Head of Department of Electrical and Electronic Engineering from 2000 to 2003 and Dean of Engineering from 2003 to 2007. His current research interests include wireless communication systems, spread spectrum techniques, CDMA and digital signal processing. He has published over 250 international journal and conference papers.

He was the General Chair of ISCAS'97 and the VP-Region 10 of IEEE CAS Society in 1999 & 2000. He was an Executive Committee Member and a Board Member of the IEE Informatics Divisional Board (1999-2001) and was an ordinary member of IEE Council (1999-2001).

He was awarded the Honorary Doctor of Engineering Degree by the University of Newcastle, Australia in 1997, the Senior Croucher Foundation Fellowship in 1999, the IEEE Third Millenium medal in 2000 and the Outstanding Researcher Award by The University of Hong Kong in 2003. He is a Fellow of IEEE, IET and HKIE.